

Journal Pre-proof

Zeolite-Graphene composite as support for Molybdenum-based catalysts and their Hydrodesulfurization performance

Islam Ali, Tawfik A. Saleh



PII: S0926-860X(20)30135-6
DOI: <https://doi.org/10.1016/j.apcata.2020.117542>
Reference: APCATA 117542

To appear in: *Applied Catalysis A, General*

Received Date: 23 November 2019
Revised Date: 21 March 2020
Accepted Date: 24 March 2020

Please cite this article as: Ali I, Saleh TA, Zeolite-Graphene composite as support for Molybdenum-based catalysts and their Hydrodesulfurization performance, *Applied Catalysis A, General* (2020), doi: <https://doi.org/10.1016/j.apcata.2020.117542>

This is a PDF file of an article that has undergone enhancements after acceptance, such as the addition of a cover page and metadata, and formatting for readability, but it is not yet the definitive version of record. This version will undergo additional copyediting, typesetting and review before it is published in its final form, but we are providing this version to give early visibility of the article. Please note that, during the production process, errors may be discovered which could affect the content, and all legal disclaimers that apply to the journal pertain.

© 2020 Published by Elsevier.

Zeolite-Graphene composite as support for Molybdenum-based catalysts and their Hydrodesulfurization performance

Islam Ali & Tawfik A. Saleh *

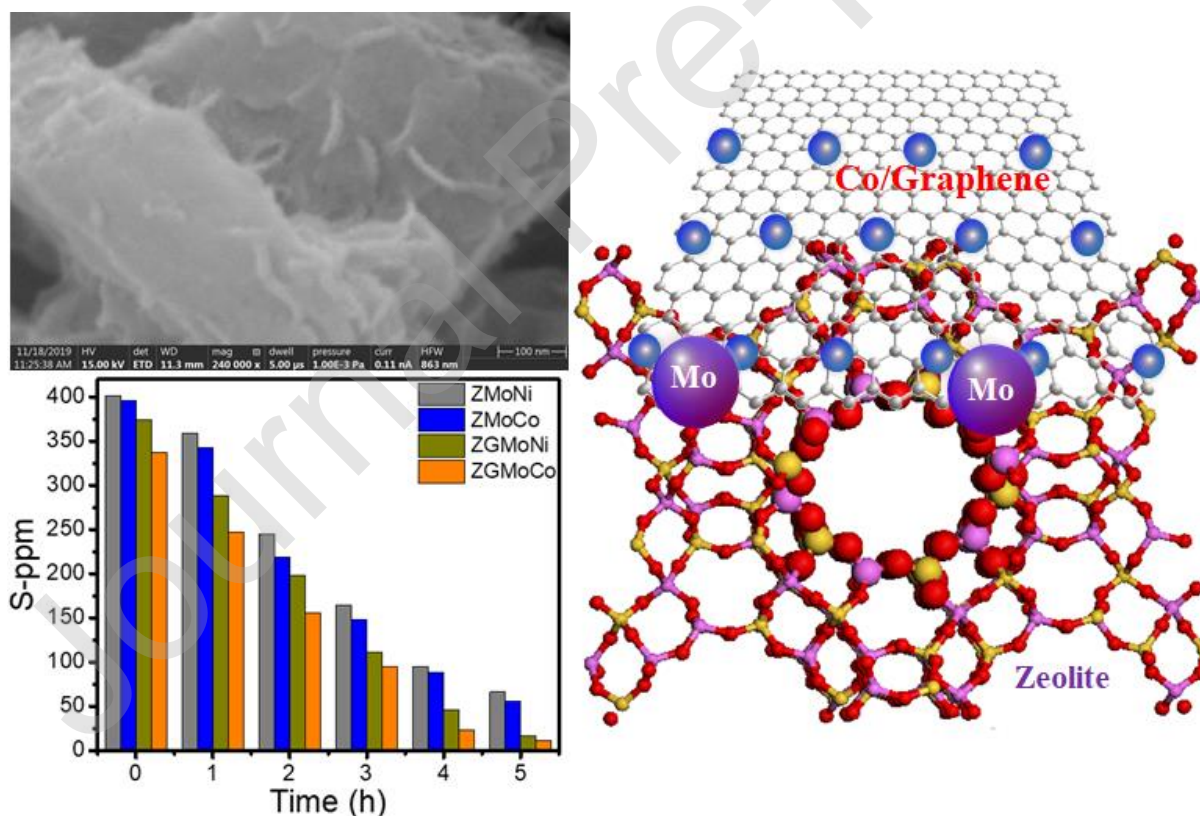
Department of Chemistry, King Fahd University of Petroleum & Minerals, Dhahran 31261,
Saudi Arabia

*Corresponding author

E-mail address: tawfik@kfupm.edu.sa ; tawfikas@hotmail.com

Home Page: <http://faculty.kfupm.edu.sa/CHEM/tawfik/publications.html>

Graphical Abstract



Highlights

- A composite of zeolite-graphene as a support decorated with molybdenum-cobalt and molybdenum-nickel were synthesized
- The ZGMC was found to reduce the sulfur content by around 98.7% after 6 h reaction time and it showed higher catalytic activity compared to the ZMC or ZMI.
- The present work is offering a convenient approach to prepare an effective HDS catalyst.

Abstract

A composite of zeolite Y type -graphene as a support doped with molybdenum-cobalt and molybdenum-nickel (active phase and promoter) was synthesized and evaluated as hydrodesulfurization (HDS) catalysts. The ZGMoCo was found to have the ability to reduce the sulfur content by $\approx 98\%$ after a 5 h reaction time which is higher compared to the ZMoCo or ZMoNi. This activity can be ascribed to the improved surface area and better distribution of the active phases (molybdenum and cobalt or nickel) on the zeolite Y type -graphene surface. SEM images showed enhanced dispersion of the active phases on the support surface. As per the BET measurements, the surface area was improved due to the introduction of graphene to be $323.6\text{ m}^2/\text{g}$ ZGMoCo compared to $257.3\text{ m}^2/\text{g}$ ZMoCo; and $312.5\text{ m}^2/\text{g}$ for ZGMoNi compared to $245.7\text{ m}^2/\text{g}$ for ZMoNi. The work offers a convenient approach to prepare an effective HDS catalyst.

Keywords: Zeolite; Graphene; Dibenzothiophene; Distribution; Hydrodesulfurization.

1. Introduction

Environmental concerns related to the fuel specifications with ultra-low sulfur content became an important approach to prevent air pollution caused by sulfur dioxide emission. Nowadays, the demand for deep desulfurization has become a requirement to meet the regulations for

sulfur in petroleum products [1-4]. Recently, sulfur content reduction in diesel fuel and gasoline by using catalytic hydrotreating has become a very intensive research area. Environmental regulation suggested that the sulfur contents in diesel and gasoline should be lowered to be 10-15 ppm [5-7]. In the refinery processes, hydrodesulfurization (HDS) has been used extensively to reduce sulfur-containing contents in petroleum. The use of hydrodesulfurization catalysts has attracted researchers owing to their good catalytic activities, product longevity, and selectivity. As a result, HDS catalysts are required to meet the specifications of sulfur during fuel transportation. Previous studies demonstrated the removal of refractory molecules like 4,6 dimethyl dibenzothiophene (4,6 DMDBT) and dibenzothiophene (DBT) which present the greatest challenge to get sulfur at ultra-low levels [8]. A highly efficient HDS catalyst with excellent properties towards desulfurization is a challenge [9-11].

The catalyst support is an important factor due to its catalytic performance [12]. To improve the hydrotreating performance of the catalyst, researchers tested zeolite and alumina. This showed that these acidic materials that contain alumina and silica mixture have a better surface area for the dispersion of metals and high concentrations of Lewis and Bronsted acid sites compared to alumina. As a result, zeolites were used extensively as a support for CoMo and NiMo [13]. The presence of a hydrogenating strong acid site has a synergetic effect, not only for accelerating the C-S bond cleavage but also for enhancing different ways of sulfur atom removal from the aromatic molecules. The microporous natural system of zeolites has a role, which limits its applications in the bulky molecules' hydrotreating field. Subsequently, the need to obtain a synthesized material with Bronsted acid sites and more surface area became of great interest [14].

Zeolite as a catalyst support is promising in the petroleum refining industry [15] because of its hierarchical structure, micro-mesoporous nature, and acid-base properties that can be

changed using synthesis methods. Zeolite was used as an adsorbent due to its capacity for ionic exchange besides its role in catalysis as a support for the dispersal of the catalyst nanoparticles [16]. Zeolite also has a role to provide acidity to the catalyst structure while the finely dispersed metal nanoparticles are used to exert hydrogenation-dehydrogenation activity. A large variety of applications are present for noble metals supported by zeolite such as the production of high-octane gasoline throughout the hydroisomerization of C₅-C₆ n-paraffins [17-18]. Also, these types of catalysts can be used in the hydrocracking process depending on the obtained product, the partial pressure of the sulphurated contaminants and the feedstock types [19]. Many types of zeolite were also included as subjects to be studied like zeolite beta (BEA) and Y zeolite-based catalyst due to their good properties as a surface for catalyst dispersion [20-23]. Supports modified with carbon such as monocarboxylic acid and citric acid have been reported to synthesize supported active metal catalysts [24-25]. These types of surface modification used to be an effective alternative way, besides the used ones [26]. For example, the intrinsic role of citric acid includes its ability to partly change to carbonaceous deposits during the sulfidation, decreasing the WS₂ slab length. It may also react with basic and neutral hydroxyl groups to moderate the interactions between the active phase and the support. The stability and catalytic performance of catalysts can be enhanced through the incorporation of nanocatalysts within suitable conductive materials. It avoids the agglomeration of the nanoparticles and accelerates charge transfer. Nickel and cobalt-based catalysts have been implemented in various applications such as HER and OER and it was used extensively as a promoter in desulfurization processes. Those materials are low cost with facile fabrication processes [27-29].

Graphene has a two-dimensional single sheet of carbon atoms distributed in a hexagonal network. It has a plate-like structure with a one-atom-thick material [30]. Due to its properties, such as a high surface area and excellent mechanical properties, it has been used in different

applications like batteries, solar cells, and composite materials, as well as catalysts [31]. One of the most characteristic features of graphene is its large specific surface area. Other properties such as mechanical, thermal and electronic features have made graphene an attractive substrate for the dispersion and deposition of nanoparticles to obtain a composite catalyst [32-33]. Recently, catalysts that use graphene as a support have become a hot area of interest [34]. Both graphene and zeolite have been implemented in various applications such as their good ability towards the molecular dye adsorption from aqueous solution. The composite fabrication for effective separation should be with a hierarchical porous structure based on zeolite or graphene. It became a promising approach for hazardous substances removal [33-38]. Also, the combination between zeolite and graphene was used extensively for the electrochemical detection of various compounds like dopamine and ascorbic acid [39] and as invitro drug carrier for anticancer drug [40].

Catalyst structure, surface atomic arrangement, and coordination are very sensitive parameters involved in catalytic reactions. Control of these parameters occurred by tuning the morphology, composition and catalyst size. The catalytically active components are bonded to support with a large surface area like alumina, zeolite, and others to confirm its dispersion on the support surface [41-44]. Different alternative supports have been used for HDS reactions such as MgO [5], SiO₂ [8], ZrO₂ [12], Al₂O₃ [4], and mixed oxides [5]. The role of supports to disperse the active phases on its surface has still not been thoroughly investigated [6].

Here, zeolite Y type - molybdenum- nickel (cobalt) (ZMoNi or ZMoCo) and Zeolite Y type - graphene/ molybdenum- nickel (cobalt) (ZGMoNi or ZGMoCo) were synthesized to illustrate the effective role of graphene for enhancing the catalyst activity. The performance of the synthesized catalyst has been investigated in catalytic reactions using desulfurization of dibenzothiophene. The structural and morphological properties of the prepared catalyst and

the role of graphene for improving the catalyst activity were characterized by different techniques.

2. Experimental

2.1. Chemicals

Commercial zeolite Y type, polyvinylpyrrolidone (C_6H_9NO)_n, decalin (>99 % purity), dibenzothiophene (DBT) (98%), ammonium molybdate tetrahydrate (98 %), cobalt nitrate hexahydrate (98%), nickel acetate tetrahydrate (98%), and ethanol (99%) were purchased from Sigma Aldrich, Eschenstrasse, Taufkirchen, Germany. De-ionized water with high purity distilled with a Labstrong FiSTREEM™ II 2S Glass Still distiller, USA and acquired in-house using Thermo-Scientific Barnstead Nanopure.

2.2. Preparation of the catalyst

Composite support of zeolite Y type -graphene (ZG) was obtained by mixing graphene dispersed in water and commercial zeolite (Y type). The sol-gel method has been used to mix around 20 mg of graphene dispersed in water with 6.4g of zeolite. During this process, 100 ml of deionized water and 0.2 g of polyvinylpyrrolidone were added to enhance the interaction between the two supports beside its role for dispersing the active phase and 10 ml ethanol was added to ZG. The stirring of the composite support was for 1 h and refluxing 5 h at 110 °C. After cooling, the filtration was performed and the product was then dried at 90 °C.

The incipient wetness impregnation procedure was used for adding the active phases of molybdenum (Mo) and cobalt (Co) or nickel (Ni) nanoparticles to the support with ratios of 15 % Mo and 5 % Co (Ni), respectively. The selection of these percentages for the active phases was decided after a literature survey and it was found that Co (Ni) was from 1-5 % and the catalyst was from 8-15 % [7]. A solution of cobalt nitrate (1.97g) and ammonium molybdate (2.43g) was prepared. Also, around 5.53 g of ZG support dispersed in 0.1 L of deionized water was kept under stirring at 90°C for 30 min. This is followed by mixing the

catalysts solutions with ZG support under stirring at 100°C for 5 h. Then, the catalyst was filtered and dried at 100 °C. Catalyst calcination in a pure nitrogen medium occurred at 350 °C for 3 h. When synthesizing the reference catalysts ZMoCo or ZMoNi, the same steps were used without the incorporation of graphene for comparison. Here, we should mention an important process during catalyst work which is the sulfidation process. It occurred within the reactor where molybdenum sulfidation happened after the temperature reached to optimum 300 °C that took around 3h.

2.3 Characterization techniques used for catalysts.

Several techniques were used for structural and morphology characterization. The textural properties of the catalysts including surface area, pore size distribution and pore volumes were measured by Micromeritics TriStar II PLUS surface area. Sample degassing before measurement at 150 °C for 3 h was performed to remove moistures and gasses. Then, the isotherm curves N₂ adsorption-desorption at -196 °C were obtained. The surface area was calculated from BET method while total pore volume was obtained by nitrogen adsorption and the pore size was attained from BJH method and its adsorption isotherm. Function groups of the catalysts were characterized by Nicolet 6700 spectrometer (Thermo Scientific) fourier transform infrared (FTIR) with a deuterated triglycine sulfate detector. A very small quantity of the material was mixed with KBr powder to prepare a thin translucent disc for measurement. The background noises correction was done using 16 scans with resolution 2 cm⁻¹. Crystallinity was recorded using Rigaku Mini-flex II x-ray diffraction (XRD). The radiation of Cu-K α was used in the 2 θ range (5-80°) and detector angular speed of 2° /min and step size of 0.02°. The surface morphology was recorded using a scanning electron microscopy (SEM) with mode name JEOL e JSM6610LV. A backscattered electron (BSE) and a secondary electron (SE) mode at an accelerating voltage of 20 kV were used. The elemental composition and sample mapping were measured with the attached Energy

dispersive X-ray spectrometer (EDX, Oxford Inc.) detector. Catalysts' thermal stability at high temperature was investigated through thermogravimetric analysis (TGA) with a model name of Q600 Thermal Analyzer Instrument. The sample heating started from ambient temperature up to 900 °C using Platinum/ Platinum Rhodium (Type R) thermocouples. The binding energies and chemical states were measured by x-ray photoelectron spectroscopy (XPS) with a model name PHI 5000 Versa Probe II, ULVAC-PHI Inc. spectroscope. A high vacuum for the disc pelletized form of the catalyst was applied before the XPS analysis start. The sample components were defined through gas chromatography-mass spectrometric technique (GC-MS) with model name Shimadzu GC17A/GC14C using quadrupole ion-trap analyzer, ions with m/z values orbits around the cavity.

2.4 Assessment of the catalysts

A batch reactor (model 4848B) from Parr instruments co. Moline, Illinois USA, was used to assess the catalyst activity (ZMoNi, ZMoCo, ZGMoNi, and ZGMoCo) towards the hydrodesulfurization of dibenzothiophene. Decalin acted as a solvent model fuel for dissolving DBT to make a feedstock solution for HDS of DBT that has 0.5 % of sulfur. The catalytic reaction conditions were 55 bars for hydrogen partial pressure and 300 °C as a reaction temperature. About 0.6 g of the synthesized catalysts interacted with 0.1L decalin and 550 ppm-S DBT. The reaction started when inserting the mixture into the vessel of the reactor. A collection of six samples and a zero point (first sample) was taken after the temperature of the reaction reached 300 °C. Reaction monitoring during 5 h was mandatory with collecting a sample every hour by a manual valve. The determination of the sulfur concentration for the collected samples was carried out by a gas-chromatography sulfur chemiluminescence detector (GC-SCD), (column: J&W 123-1033 - DB-1, 30m, 0.32mm, 1.00um). Agilent Stevens Creek Blvd. Santa Clara, United States. GC-MS technique was implemented to illustrate the components of the synthesized catalysts.

3. Results and discussion

3.1. Physico-chemical properties

The N₂ sorption isotherms and distribution of pore size of the catalysts were conducted, **Fig. S1**. The textural properties of the catalysts are illustrated in **Table 1**. Incorporation of graphene within zeolite Y type to form composite support increased the surface area from 245.7 m²·g⁻¹ (ZMoNi) to 312.5 m²·g⁻¹ (ZGMoNi) and from 257.3 m²·g⁻¹ (ZMoCo) to 323.6 m²·g⁻¹ (ZGMoCo) and. This improvement in the surface area enhances the activity of the catalysts. Also, the improvement was attributed to the quantity of graphene after parameter optimization for commercialization purposes. The isotherm curves are like type IV. At a high value of relative pressure, there is a hysteresis loop which clarifies the mesoporous nature of the material, while the nitrogen uptake at low pressures indicated the microporous existence within the catalysts. Therefore, graphene improved the textural properties of the catalysts that lead to an enhanced activity towards the hydrodesulfurization of benzothiophenes. It was found the slight change in the textural properties of the catalyst ZGMoCo after HDS reaction that prove the stability of the catalyst.

The hierarchy factor (HF) was also calculated to illustrate the role of graphene on the textural properties of the catalysts as:

$$HF = (V_{\text{micro}}/V_{\text{total}}) * (S_{\text{meso}}/S_{\text{BET}}) \quad (1)$$

By replacing these parameters in Eq. (1), the HF was obtained. It was shown that the HF values for ZGMoNi and ZGMoCo are higher than the reference sample ZMoNi and ZMoCo which clarifies their higher adsorption efficiency [8]. The quantity adsorbed-desorbed for catalysts was always higher than the reference one at any relative pressure value, which supports our results regarding HF.

The incorporation of graphene into the catalyst component has a crucial effect on its stability. TGA curves, **Fig. S2**, indicated that in the temperature range 0-900 °C and inert gas medium, it is obvious that the weight loss for the ZMoNi reference sample was 17 % at 400 °C and 27 % at 800 °C, while for ZGMoNi, it was 13 % at 400 °C and was reduced by only 4 % up to 800 °C. In addition, the weight loss for ZMoCo was 14.6 % at 400 °C and 23 % up to 800 °C, compared to ZGMoCo which was 11 % and 18 % for the same temperature scale. The total decomposition rate of ZGMoNi and ZGMoCo after 800 °C was 18.9 % and 17 %, which is better than the reference ones (ZMoNi and ZMoCo) that were 22.5 % and 27 %. These results reflected the enhanced thermal stability of the synthesized catalyst after graphene incorporation into the zeolite Y type.

The XRD patterns for the synthesized catalysts, **Fig. S3**, indicated that the characteristic peak at $2\theta = 27.3^\circ$ (100) was attributed to MoO_3 according to JCPDS card no. 05-0508. Peaks at $2\theta = 6.3^\circ$ (002), 19.2° (006), 21.3° (101), 24.6° (104), 32.7° (108), 35.6° (112) can be assigned to zeolite material that appeared in the four catalysts. No clear peaks for the active phases Mo and Co (Ni) could be due to their enhanced dispersion on the composite support surface which is consistent with the nitrogen adsorption-desorption results. In the modified catalyst, no diffraction peak for graphene appeared in the curve, which may be due to the low diffraction intensity of graphene and its low amount [9].

In the FTIR patterns, **Fig. S4**, reveal a slightly small peak at $\approx 3600 \text{ cm}^{-1}$ was ascribed to the bridging OH group in Al-OH-Si [8, 10]. The observed peaks at 486 and 1086 cm^{-1} were related to the Mo=O central vibrational mode [13]. Bands in the range of $450\text{-}1000 \text{ cm}^{-1}$ indicated good dispersion of the active phases on the composite support surface [11]. The band at 1566 cm^{-1} maybe for the OH bending mode.

The catalysts' surface morphologies and their elemental compositions were examined by a scanning electron microscope (SEM) and energy-dispersive x-ray spectroscopy (EDX). **Fig.**

1 illustrates the SEM images for the four catalysts. The surface modification by graphene doping enhanced the dispersion of the active phases Mo and Co (Ni) on the composite support surface. Images of ZGMoCo and ZGMoNi (5_{e-h}) show a better distribution of the catalyst and promoter on the catalyst support surface and the role of graphene sheets for enhancing the surface area. From these images, graphene sheets are present beside the zeolite support. In comparison to the reference samples, it was noticed in the ZMoNi and ZMoCo images (5_{a-d}), that the dispersion of the active phase is poor and not homogenous [18]. The catalyst SEM image was presented in (5_{i-j}) and it does not show a big difference from the catalyst before HDS reactions. EDX spectra were used to confirm the presence of elements introduced into the catalysts' composition. The existence of all the elements Al, Si, Co, Mo, and nickel were confirmed in the reference samples, **Fig. 1**, while the carbon element attributed to the graphene incorporation. Consequently, we successfully introduced support and active phases into the four catalysts. HRSEM and mapping were utilized to evaluate the distribution and introduction of the components in the ZGMoCo catalyst, **Fig. 2**. It was shown that all the components have been induced within the catalyst with a homogenous dispersion.

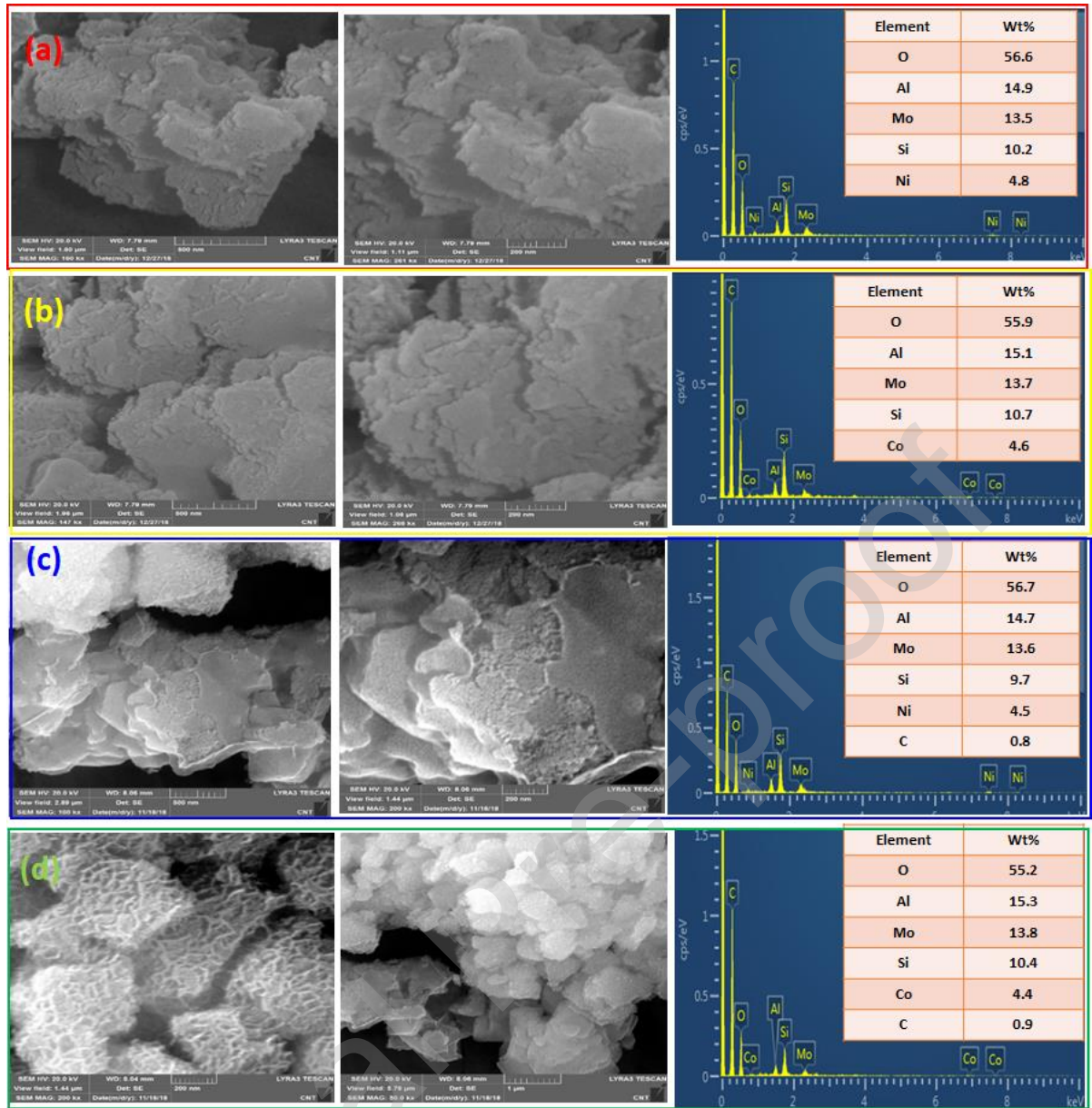


Fig. 1. SEM Images and EDX spectra of ZMoNi (a), ZMoCo (b), ZGMoNi (c), and ZGMoCo (d)

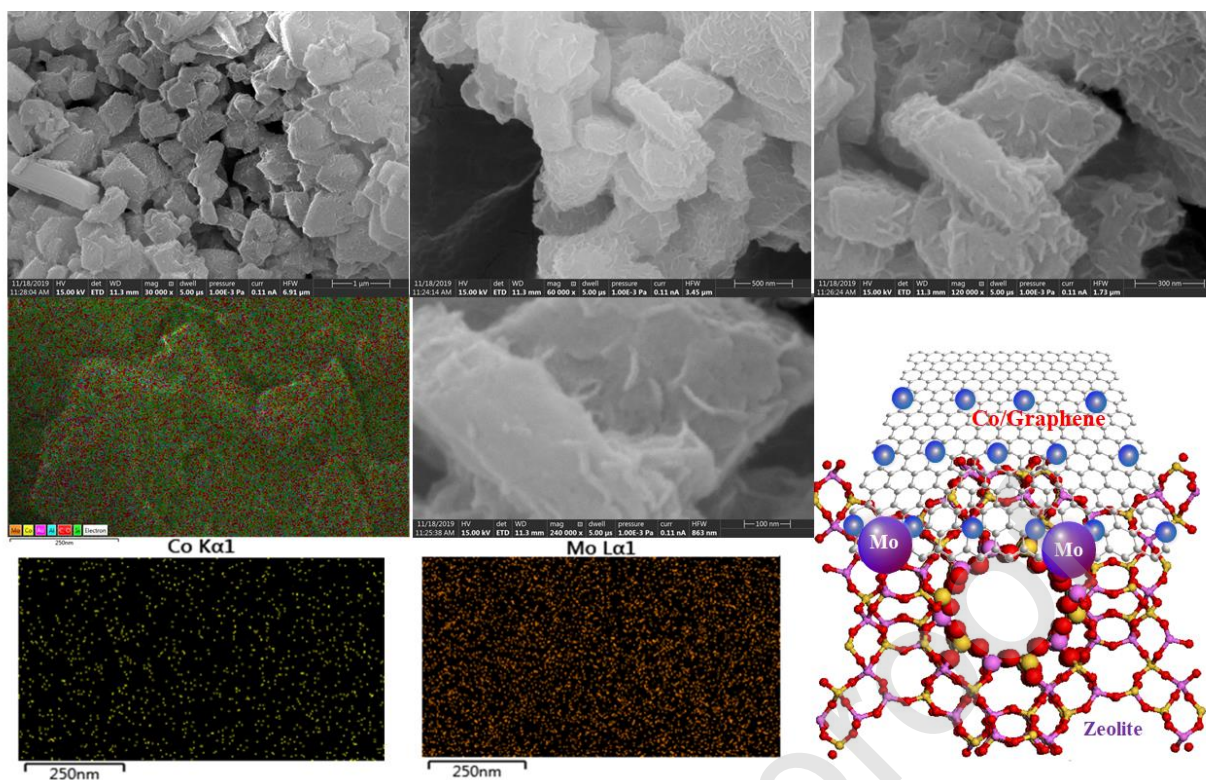


Fig. 2. HRSEM and illustration of the structure and Mapping of the ZGMoCo catalyst

The surface study regarding chemical states and binding energies of the catalyst components was discussed using XPS in **Fig. 3**, and **Table (2)**. The fully scanned spectrum proved the presence of many elements in the synthesized catalyst. Some insights and identification for the degree of Mo species sulfidation [39]. The characteristic binding energies of Mo oxide species were illustrated as per deconvoluted XPS spectra. The spectra confirmed the presence of MoO_2 (Mo^{4+} ($3d_{5/2}$)) and MoO_3 (Mo^{6+} ($3d_{5/2}$) and Mo^{6+} ($3d_{3/2}$) at 230.3 eV, 232.7 eV and 235.8 eV respectively. The peaks in the range 775-786 eV was related to Co2p [41-42]. The characteristic peak for C1s which is located at 284.7 eV reflected the graphitized structure [43]. The peak at 529 eV was attributed to O1s that contribute to Mo-O and O of MoO_3 exists in the form of O^{2-} [44].

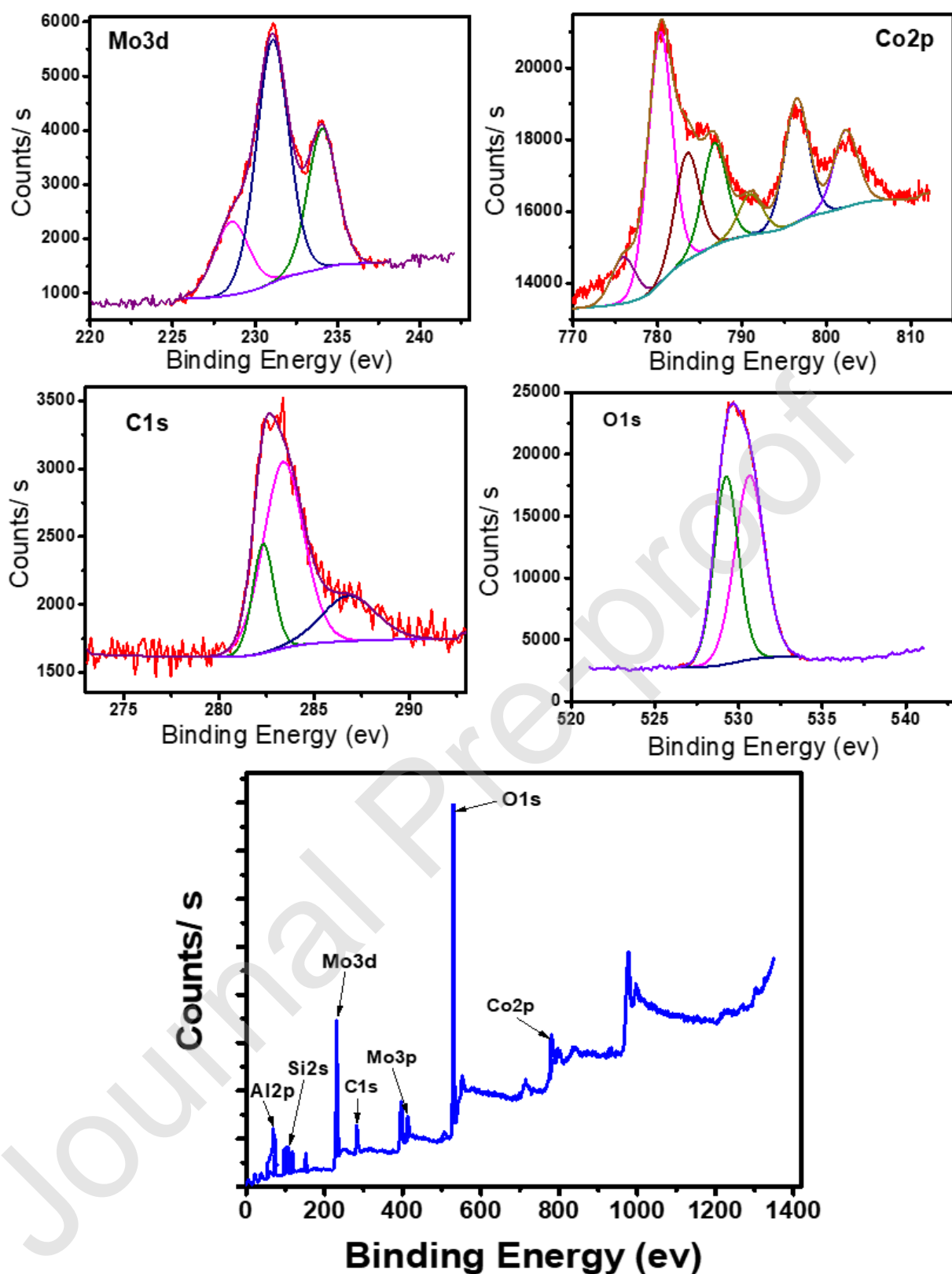


Fig. 3. XPS spectra of Mo3d, Co2p, C1s and O1s for the catalyst ZGMoCo.

3.2. Catalysts activity towards HDS

Fig. 4 and 5 show the sulfur conversion in ppm for 5 h reaction time and the percent of this value for the mentioned four catalysts. The reaction parameters used for DBT desulfurization were 300 °C temperature, H₂ partial pressure of 55 bar, rotation of 190 rpm, catalyst amount (0.6 g), and 0.1 L model fuel. It was noted that after 5 h, the sulfur concentration for the reference samples ZMoNi and ZMoCo were 66.3 and 55.8 ppm, respectively, while the modified catalyst showed enhanced sulfur removal to be 16.7 and 11.2 ppm for ZGMoNi and ZGMoCo respectively. The conversion percentage for the catalysts is illustrated in Fig. 5. It was 89.8 %, 91.4 %, 97.5 and 98.3 % for ZMoNi, ZMoCo, ZGMoNi and ZGMoCo, respectively, Table S1,2. The improvement in the surface area of the catalyst after the incorporation of graphene has a crucial role in increasing the catalytic activity. Also, the HF calculation and adsorption-desorption isotherm supported our conclusion regarding the activity. All the textural properties like pore volume and surface area with average pore diameter were enhanced with graphene doping which leads to a better distribution of the active phases on the composite support surface.

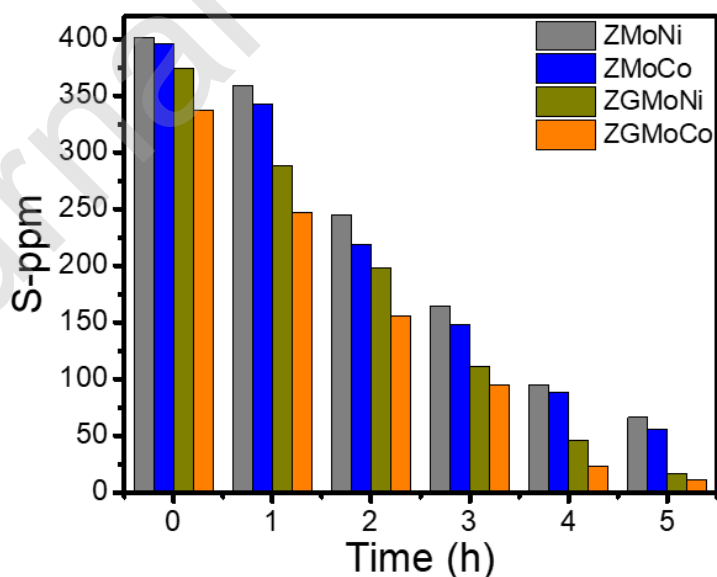


Fig. 4. Catalytic activity of the prepared catalysts in ppm sulfur

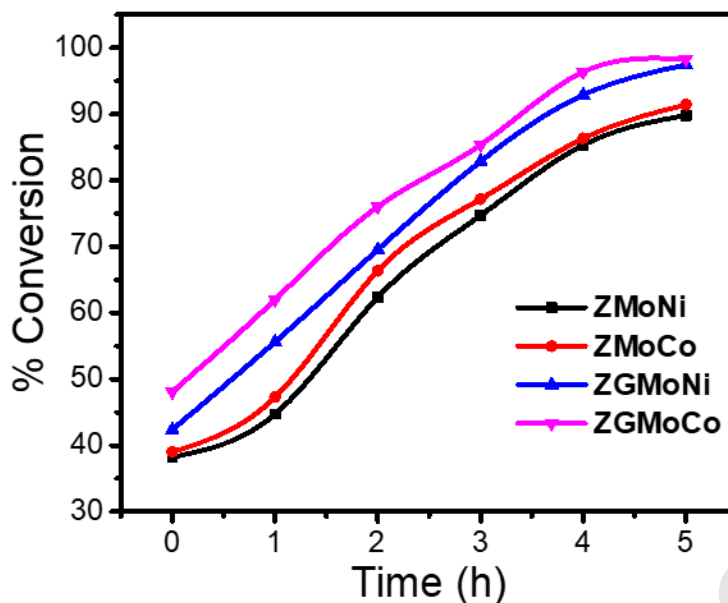


Fig. 5. Percentage of conversion using the prepared catalysts

3.3. Proposed reaction mechanism for hydrodesulfurization

There are two routes for sulfur removal from DBT, namely, hydrogenation (HYD) and hydrogenolysis or direct desulfurization (DDS), as in Fig. 6. In the case of hydrogenation, tetrahydro and hexahydro DBT were obtained as intermediate products for DBT. Then, desulfurization occurred to form cyclohexyl benzene and finally bicyclohexyl, while, in the DDS route, no intermediate products are formed as DBT was desulfurized directly to form biphenyl. The reaction pathway of DBT hydrodesulfurization over the synthesized catalysts is proposed in Fig. 7. Product analysis in GC-MS was used to illustrate the proposed pathway. It was expected to be hydrogenolysis as DBT was desulfurized by C-S bond breaking to obtain biphenyl (BP). The presence of a hydrogen source leads to the hydrogenation of biphenyl to get cyclohexyl benzene (CHB). The large number of peaks in GC-MS may be attributed to the high number of products that were separated for each analysis, Fig. S5. The characteristic peak at 154 m/z is related to biphenyl, while the peak at 166 m/z was attributed to bicyclohexyl. As a conclusion from these results, the direct desulfurization pathway can be a dominant path for DBT over the ZGMoCo catalyst. The percent distribution of the compounds

biphenyl, cyclohexyl benzene, tetrahydro dibenzothiophene and hexahydro dibenzothiophene were listed in Table S3, it was shown that the contribution of the intermediate products THDBT and HDDBT is very low while the ratio of CHB and BP is high to confirm the conclusion regarding the dominance of DDS pathway as the main one for hydrodesulfurization of DBT [45-47].

In **Fig. 7**, structural interactions are proposed between graphene and zeolite, in addition to the combination of the active phases and the composite support surface. As a final step, C-S bond breaking and releasing of biphenyl from DBT. The existence of hydrogen during HDS lead to the formation of bicyclohexyl. A comparison of our catalyst with literature was made and presented in **Table 3**.

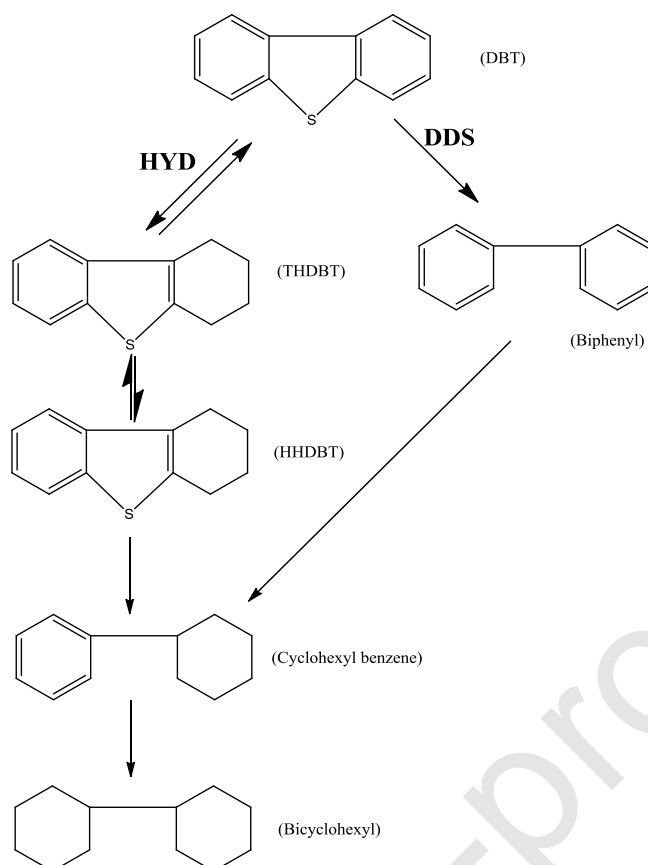


Fig. 6: A proposed route for DBT hydrodesulfurization

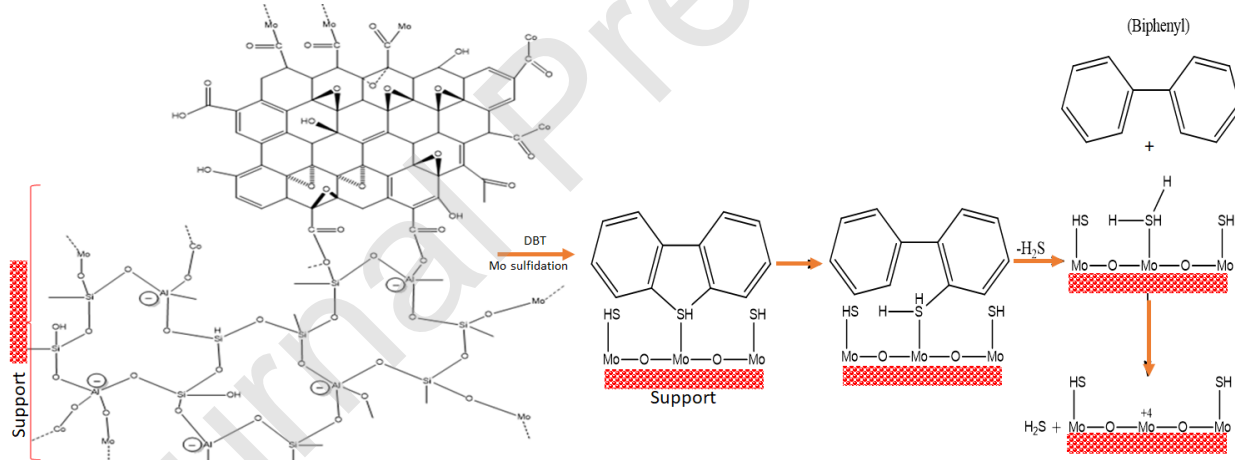


Fig. 7. Proposed mechanism for the interaction between the composite support and active phases.

Conclusion

The results in this work showed the higher activity of zeolite Y type -graphene/ molybdenum - cobalt (nickel) compared to zeolite Y type / molybdenum-cobalt (nickel) for dibenzo thiophene hydrodesulfurization reactions. Data obtained for the synthesized catalyst showed

an improvement in the textural properties like surface area and pore size after doping graphene as a co-support with zeolite Y type. The SEM images illustrated the enhanced dispersion of the active phases on the support surface in the presence of graphene. TGA indicated the improved thermal stability of the synthesized catalyst, as the percentage weight loss for the four catalysts has been reduced after graphene incorporation within the support. The EDX results confirmed the successful introduction of the nanoparticles' active phase on the support surface. The novel catalysts ZGMoCo and ZGMoNi evaluation for the desulfurization of DBT was found to be superior when compared to the reference samples ZMoCo and ZMoNi. The catalyst activity was $\approx 98\%$ (ZGMoCo) removal of sulfur compared to 91.4% (ZMoCo) and 97.5% (ZGMoNi) to 89.8% (ZMoNi). Regarding the mechanism pathway involved during the HDS reaction, it was found to be direct desulfurization as per the obtained data from GC-MS. In conclusion, we confirmed the effective role of graphene doping within the catalyst to form composite support. The superior activity for sulfur removal with enhanced properties was also obtained.

Author contribution

Islam Ali performed the experiments and results. Tawfik A. Saleh reviewed the paper and checked the manuscript.

References

- [1] M.I. Mohammed, A.A. Abdul, R. Mohammed, Synthesis of nanocatalyst for hydrodesulfurization of gasoil using laboratory hydrothermal rig, Arab. J. Sci. Eng. (2017) 1381-1387.
- [2] P. Schacht, G. Hernández, L. Cedeño, J.H. Mendoza, S. Ramírez, L. García, J. Ancheyta, Hydro-desulfurization activity of CoMo catalysts supported on stabilized TiO₂, Energy Fuels 17 (2003) 81-86.
- [3] Gutiérrez OY, Fuentes GA, Salcedo C, Klimova T. SBA-15 supports modified by Ti and Zr grafting for NiMo hydrodesulfurization catalysts. Catal Today 2006; 116: 485-497.
- [4] Laurenti D, Ngoc BP, Roukoss C, Devers E, Marchand K, Massin L, Lemaitre L, Legens C, Quoineaud AA, Vrinat M. Intrinsic potential of alumina-supported CoMo catalysts in HDS: Comparison between γ c, γ t, and δ -alumina. J Catal 2013; 297: 165-175.

- [5] Mbarki R, Mnif A, Hamzaoui AH. Structural, dielectric relaxation and electrical conductivity behavior in MgO powders synthesized by sol-gel. *Mater Sci Semicond Process* 2015; 29: 300-306.
- [6] Kaluža L, Gulková D, Vít Z, Zdražil M. High-activity MgO-supported CoMo hydrodesulfurization catalysts prepared by non-aqueous impregnation. *Appl Catal B Environ* 2015; 162: 430-436.
- [7] Zhang Q, Qian W, Oshima S, Ishihara A, Kabe T. the role of cobalt on hydrodesulfurization and hydrogenation of dibenzothiophene and 4,6-dimethyldibenzothiophene catalyzed by Co-Mo/Al₂O₃, *Sekiyu Gakkaishi. J Japan Pet Inst* 1997; 40: 408-414.
- [8] Ramírez JP, Verboekend D, Bonilla A, Abelló S. Zeolite catalysts with tunable hierarchy factor by pore-growth moderators. *Adv Funct Mater* 2009; 19: 3972-3979.
- [9] A. Nezamzadeh-ejhieh, A. Shirzadi, Chemosphere Enhancement of the photocatalytic activity of Ferrous Oxide by doping onto the nano-clinoptilolite particles towards photodegradation of tetracycline, *Chemosphere*. 107 (2014) 136-144.
- [10] S. Jafari, A. Nezamzadeh-ejhieh, supporting of coupled silver halides onto clinoptilolite nanoparticles as simple method for increasing their photocatalytic activity in heterogeneous photodegradation of mixture of 4-methoxy aniline and 4-chloro-3-nitro aniline, *J. Colloid Interface Sci.* 490 (2017) 478-487.
- [11] AL-Hammadi, S. A., Al-Amer, A. M., & Saleh, T. A. (2018). Alumina-carbon nanofiber composite as a support for MoCo catalysts in hydrodesulfurization reactions. *Chemical Engineering Journal*, 345(January), 242–251.
- [12] Jia M, Afanasiev P, Vrinat M. The influence of preparation method on the properties of NiMo sulfide catalysts supported on ZrO₂. *Appl Catal A Gen* 2005; 278:213-221. .
- [13] Amezcua JC, Lizama L, Salcedo C, Puente I, Domínguez JM, Klimova T. NiMo catalysts supported on titania-modified SBA-16 for 4,6-dimethyldibenzothiophene hydrodesulfurization. *Catal Today* 2005; 107–108: 578-588.
- [14] Pérot G. Hydrotreating catalysts containing zeolites and related materials - Mechanistic aspects related to deep desulfurization. *Catal Today* 2003; 86:111-128.
- [15] Degnan TF, Jr. Applications of zeolites in petroleum refining. *Top Catal* 2000; 13:349-356
- [16] Akhmedov V, Al-Khowaiter S. Recent advances and future aspects in the selective isomerization of high n-alkanes. *Catal Rev Sci Eng* 2007; 49: 33-139.
- [17] Zhang Q, Deng W, Wang Y. Recent advances in understanding the key catalyst factors for Fischer-Tropsch synthesis. *J Energy Chem* 2013; 22: 27-38.
- [18] Heracleous E, Iliopoulou EF, Lappas AA. Microporous/mesoporous Pt/ZSM-5 catalysts for hydroisomerization of BTL-naphtha. *Ind Eng Chem Res* 2013; 52:14567-14573.
- [19] Mendes PSF, Lapisardi G, Bouchy C, Rivallan M, Silva JM, Ribeiro MF. Hydrogenating activity of Pt/zeolite catalysts focusing acid support and metal dispersion influence. *Appl Catal A Gen* 2015; 504: 17-28.
- [20] Deldari H. Suitable catalysts for hydroisomerization of long-chain normal paraffins. *Appl Catal A Gen* 2005; 293:1-10.
- [21] Park KC, Ihm SK. Comparison of Pt/zeolite catalysts for n-hexadecane hydroisomerization. *Appl Catal A Gen* 2000; 203:201-209.
- [22] Gutiérrez A, Arandes JM, Castaño P, Olazar M, Bilbao J. Preliminary studies on fuel production through LCO hydrocracking on noble-metal supported catalysts. *Fuel* 2012; 94: 504-515
- [23] Zhang W, Smirniotis PG. Effect of zeolite structure and acidity on the product selectivity and reaction mechanism for n-octane hydroisomerization and hydrocracking. *J Catal* 1999; 182:400-416.

- [24] Wei MJ, Zhou J, Lu X, Zhu Y, Liu W, Lu L, Zhang L. Diffusion of water molecules confined in slits of rutile TiO₂(110) and graphite (0001). *Fluid Phase Equilib* 2011; 302:316-320.
- [25] Li H, Li M, Chu Y, Liu F, Nie H. Essential role of citric acid in preparation of efficient NiW/Al₂O₃HDS catalysts. *Appl Catal A Gen* 2011; 403:75-82.
- [26] Li L, Wang Y, Shi K, Chen S, Yang Z, Lu X. Preparation and characterization of mesoporous MoO₃/TiO₂ composite with high surface area by self-supporting and ammonia method. *Catal Lett* 2012; 142:480-485.
- [27] Guo, X., Kong, R. M., Zhang, X., Du, H., & Qu, F. (2018). Ni(OH)₂ Nanoparticles Embedded in Conductive Microrod Array: An Efficient and Durable Electrocatalyst for Alkaline Oxygen Evolution Reaction. *ACS Catalysis*, 8(1), 651-655.
- [28] Pena, L., Valencia, D., Klimova, T., 2014. CoMo/SBA-15 catalysts prepared with EDTA ~ and citric acid and their performance in hydrodesulfurization of dibenzothiophene. *Appl. Catal. B Environ.* 147, 879-887.
- [29] Hubaut, R., Altafulla, J., Rives, A., Scott, C., 2007. Characterization and HDS activities of mixed FeMo sulphides supported on alumina and carbon. *Fuel* 86, 743-749.
- [30] Stoller MD, Park S, Zhu Y, An J, Ruoff RS. Graphene-Based Ultracapacitors. *Nano Lett* 2008; 8: 3498-3502.
- [31] Kamat PV. Graphene-based nanoassemblies for energy conversion. *J Phys Chem Lett* 2011; 2:242-251.
- [32] MacHado BF, Serp P. Graphene-based materials for catalysis. *Catal Sci Technol* 2012; 2: 54-75.
- [33] Zhou Q, Zhao Z, Zhang Y, Meng B, Zhou A, Qiu J. Graphene sheets from graphitized anthracite coal: Preparation, decoration, and application. *Energy & Fuels* 2012; 26: 5186-5192.
- [34] Zhu L, Zhang S, Cui Y, Song H, Chen X. One step synthesis and capacitive performance of graphene nanosheets/Mn₃O₄ composite. *Electrochim Acta* 2013; 89: 18-23.
- [35] Yu, Y., Murthy, B. N., Shapter, J. G., Constantopoulos, K. T., Voelcker, N. H., & Ellis, A. V. (2013). Benzene carboxylic acid derivatized graphene oxide nanosheets on natural zeolites as effective adsorbents for cationic dye removal. *Journal of Hazardous Materials*, 260, 330-338.
- [36] Saeidi, N., Parvini, M., & Niavarani, Z. (2015). High surface area and mesoporous graphene/activated carbon composite for adsorption of Pb(II) from wastewater. *Journal of Environmental Chemical Engineering*, 3(4), 2697-2706.
- [37] Fan, Q., Yang, Y., Hao, Y. K., Zhao, X., & Feng, Y. (2015). Preparation of three-dimensional PANI/GO for the separation of Hg(II) from aqueous solution. *Journal of Molecular Liquids*, 212, 557-562.
- [38] Ai, L., & Jiang, J. (2012). Removal of methylene blue from aqueous solution with self-assembled cylindrical graphene-carbon nanotube hybrid. *Chemical Engineering Journal*, 192, 156-163.
- [39] He, P., Wang, W., Du, L., Dong, F., Deng, Y., & Zhang, T. (2012). Zeolite A functionalized with copper nanoparticles and graphene oxide for simultaneous electrochemical determination of dopamine and ascorbic acid. *Analytica Chimica Acta*, 739, 25-30.
- [40] Khatamian, M., Divband, B., & Farahmand-Zahed, F. (2016). Synthesis and characterization of Zinc (II)-loaded Zeolite/Graphene oxide nanocomposite as a new drug carrier. *Materials Science and Engineering C*, 66, 251-258.
- [41] J. Xu, Y. Guo, T. Huang, Y. Fan, Hexamethonium bromide-assisted synthesis of CoMo/graphene catalysts for selective hydrodesulfurization, *Appl. Catal. B Environ.* 244 (2019) 385–395.

- [42] H. Wu, A. Duan, Z. Zhao, D. Qi, J. Li, B. Liu, G. Jiang, J. Liu, Y. Wei, X. Zhang, Preparation of NiMo/KIT-6 hydrodesulfurization catalysts with tunable sulfidation and dispersion degrees of active phase by addition of citric acid as chelating agent, *Fuel* 130 (2014) 203–210.
- [43] Yu F, Ma J and Wu Y, Adsorption of toluene, ethylbenzene and m-xylene on multi-walled carbon nanotubes with different oxygen contents from aqueous solutions. *J Hazard Mater* 192:1370–1379 (2011).
- [44] Li Y, Wei X, Yan X, Cai J, Zhou A, Yang M et al., Construction of inorganic–organic 2D/2D WO₃/g-C₃N₄ nanosheet arrays toward efficient photoelectrochemical splitting of natural seawater. *Phys Chem Chem Phys* 18:10255–10261 (2016).
- [45] V.C. Srivastava, An evaluation of desulfurization technologies for sulfur removal from liquid fuels, *RSC Advances*, (2012) 759-783.
- [46] H. Li, W. Zhu, S. Zhu, J. Xia, Y. Chang, W. Jiang, M. Zhang, Y. Zhou and H. Li, the selectivity for sulfur removal from oils: An insight from conceptual density functional theory, *AIChE J.*, 62 (2016) 2087–2100.
- [47] H. Liu, C. Yin, B. Liu, X. Li, Y. Li, Y. Chai, C. Liu, Effect of calcination temperature of unsupported NiMo catalysts on the hydrodesulfurization of dibenzothiophene, *Energy and Fuels*. 28 (2014) 2429–2436.
- [48] Pedernera, E., Reimert, R., Nguyen, N.L., Van Buren, V., 2003. Deep desulfurization of middle distillates: process adaptation to oil fractions' compositions. *Catal. Today* 79e80, 371-381.
- [49] T. Kabe, W. Qian, S. Ogawa, A. Ishihara, Mechanism of hydrodesulfurization of dibenzothiophene on CoMoAl₂O₃ and CoAl₂O₃ catalyst by the use of radioisotope ³⁵S tracer, *J. Catal.* 143 (1993) 239–248,
- [50] Kunisada, N., Choi, K.H., Korai, Y., Mochida, I., 2004. Effective supports to moderate H₂S inhibition on cobalt and nickel molybdenum sulfide catalysts in deep desulfurization of gas oil. *Appl. Catal. A Gen.* 260, 185-190.
- [51] Da Costa, P., Manoli, J., Potvin, C., 2005. Deep HDS on doped molybdenum carbides: from probe molecules to real feedstocks. *Catal. Today* 108, 520-530.

Table 1: Textural properties of the prepared catalysts

Items	ZMoNi	ZMoCo	ZGMoNi	ZGMoCo	ZGMoCo after HDS
BET surface area ($\text{m}^2 \cdot \text{g}^{-1}$)	245.7	257.3	312.5	323.6	324.7
Microporous surface area ($\text{m}^2 \cdot \text{g}^{-1}$)	193.8	198.6	251.3	248.8	253.6
External surface area ($\text{m}^2 \cdot \text{g}^{-1}$)	51.9	58.7	61.2	74.8	71.1
Microporous pore volume ($\text{m}^3 \cdot \text{g}^{-1}$)	0.0078	0.0091	0.0096	0.0095	0.0093
Average pore size (nm)	3.5	3.8	3.2	3.6	3.6
Total Pore volume ($\text{m}^3 \cdot \text{g}^{-1}$)	0.23	0.24	0.18	0.21	0.22
Hierarchy factor (HF)	0.016	0.019	0.025	0.027	0.028

Table 2: XPS data for the catalyst ZGMoCo

Elements	BE (ev)	FWHM
Mo3d (Mo ⁴⁺ (3d _{5/2}))	230.3	2.5
Mo3d (Mo ⁶⁺ (3d _{5/2}))	232.7	2.3
Mo3d (Mo ⁶⁺ (3d _{3/2}))	235.8	2.1
Co2p	785.2	3.4
O1s	531	1.7
C1s	284.7	1.3

Table 3: Comparison between the catalytic activity of ZGMoCo and other reported catalysts.

Catalysts	Sulfur concentration (ppm)	Sulfur removal (%)	References
ZGMoCo	550 ppm	≈98 %	Current work
NiMo/Al ₂ O ₃	740 ppm	90 %	[48]
Co-Mo/Al ₂ O ₃	4000 ppm	67 %	[49]
CoMoS and NiMoS	340 ppm	97 %	[50]
P and Ni-Al ₂ O ₃ supported Mo oxycarbide	520 ppm	50 %	[51]
CoMo/SBA-15	2160 ppm	77 %	[28]
FeMoS/Carbon	1000 ppm	30 %	[29]
MoCo/CNT	1300 ppm	73.5 %	[1]
CoMo/TiO ₂	300 ppm	60.5 %	[2]